第35卷 第4期 焊 接 学 报 Vol. 35 No. 4
2014年4月 TRANSACTIONS OF THE CHINA WELDING INSTITUTION April 2014

高强焊丝熔敷金属力学性能及组织分析

吴炳智， 徐玉君， 安洪亮， 孙静涛
(机械科学研究院 哈尔滨焊接研究所，哈尔滨 150028)

摘 要：利用金相显微镜、扫描电子显微镜(SEM)及附带能谱仪(EDS)并通过常温拉伸和低温冲击等试验研究了不同保护气体下高强焊丝熔敷金属组织和强韧性变化. 结果表明，针对此高强度气体保护焊焊丝，采用 Ar + 5% CO_2 保护气体，熔敷金属强韧性最佳；焊缝金相组织为粒状贝氏体 + 板条贝氏体，细小板条束可有效提高焊缝韧性；M-A 组元存在明显 C 元素富集的现象，大量块状 M-A 组元的出现造成 M-A 组元基体间位错塞积，引起应力集中，在裂纹形核阶段易萌生微裂纹，对韧性不利；采用 Ar + 2% O_2 和 Ar + 20% CO_2 保护气体，焊缝中较大尺寸夹杂物数量增多，是诱发准解理断裂引起冲击吸收功降低的主要原因.

关键词：高强钢；熔敷金属；力学性能；组织
中图分类号：TG 422.3 **文献标识码**：A **文章编号**：0253 - 360X(2014)04 - 0053 - 05

0 序 言

由于高强钢具有可减轻结构自重、增强结构可靠性、提高工程机械工作效率及使用寿命和降低原材料消耗等优点被广泛应用于各工程领域，且随着新的冶炼技术和强化途径，高强钢强度级别也不断提高，越来越多的行业对钢的强度和韧性提出了更高的要求，如采油平台、舰艇、管线钢[1]和压力容器[2]等行业，而焊缝作为大型结构的重要组成部分往往是薄弱环节，为了推进新型高强度钢材的不断应用，迫切需要与之配套的高强高韧性焊接材料，与此同时研究焊缝金属的组织性能也十分重要.

众所周知，熔化金属与保护气体之间在焊接高温下的化学反应是重要的焊接冶金过程，它与焊缝金属中的化学成分、微观组织、焊接接头性能及其可靠性有很大关系，CO_2 含量对低温韧性的影响主要是通过对合金元素的含量变化、非金属夹杂物形态和氧在焊缝中的存在状态来解释 CO_2 对低温韧性的作用机理[3]，已有研究表明[4]采用混合气体保护焊焊缝中阻碍裂纹扩展的大角度晶界比例明显增加，可显著改善低温韧性. 但目前国内外的研究主要集中在较低强度级别焊缝金属，较低强度级别焊缝是以针状铁素体为主的组织，关于此类焊缝强韧化机理如细小、难溶非金属夹杂物作为一种高能惰性表面，降低形核壁垒，促进针状铁素体多维及感应形核已有较多研究[5-7]，而针对高强度级别熔敷金属组织性能研究较少. 文中重点研究了不同保护气体下熔敷金属的组织及性能，分析了微观组织、冲击吸收功及断口形貌之间的对应关系，并对熔敷金属中的夹杂物进行了定量分析，该研究对进一步研制高强度级别焊丝起到一定的指导作用.

收稿日期：2013 - 10 - 08
基金项目：高档数控机床与基础制造装备科技重大专项资助项目(2011ZX04016 - 061)

1 试验方法

试板焊接和力学性能取样参照国家标准 GB/T8110—2008《气体保护电弧焊用碳钢、低合金钢焊丝》. 试板材料选用低碳钢 Q235，尺寸为 300 mm × 120 mm × 20 mm. 焊接材料为自行设计冶炼的实心焊丝 HS-90，直径为 1.2 mm，其化学成分见表 1. 坡口设计如图 1 所示，隔离层防止母材对焊缝金属的稀释. 焊接方法选熔化极气体保护焊，焊接电源为 Fronius TPS5000 全数字化电源，焊接过程保护气体分别采用 Ar + 2% O_2，Ar + 5% CO_2 和 Ar + 20% CO_2，焊接工艺参数见表 2.

表 1 焊丝的化学成分(质量分数，%)

Table 1 Chemical compositions of solder wire

C	Si	Mn	S	P	Cr
0.062	0.71	1.86	0.004	0.004	0.38
Ni	Mo	Ti	Cu	Nb	Fe
2.16	0.6	0.05	0.18	<0.01	余量

金相试样取自焊缝截面，用砂纸研磨、抛光后，

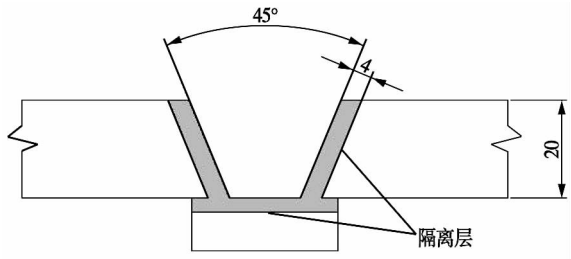

图 1 坡口示意图(mm)

Fig. 1 Schematic of groove

表 2 焊接工艺参数

Table 2 Welding parameters

焊接电流 I/A	电弧电压 U/V	焊接速度 v/(cm·min^{-1})	气体流量 q/(L·min^{-1})	道间温度 T/℃
260 ~ 280	26 ~ 30	33	20	150

采用 3% 硝酸酒精溶液腐蚀. 利用 Olympus-PME 型光学显微镜(OM)观察焊缝金相组织. 使用 FEI Sirion 200 型高分辨率场发射扫描电镜(SEM)观察焊缝微观组织及冲击断口形貌,利用附带能谱分析仪 EDS 分析 M-A 组元及夹杂物成分,通过 Image-Pro Plus 图像处理软件对夹杂物进行定量分析. 拉伸试验按照国家标准 GB/T2652—2008《焊缝及熔敷金属拉伸试验方法》进行. 冲击试验按照国家标准 GB/T2650—2008《焊接接头冲击试验方法》进行,试验温度为 -40和 -60 ℃.

2 微观组织及力学性能分析

2.1 焊缝表面成形

图 2 为不同保护气体下焊缝表面成形. 由图 2 可见试验条件下采用的 3 种保护气体配比,焊接过程 Ar + 5% CO_2 电弧稳定性最好,Ar + 20% CO_2 焊接存在少量飞溅,三者均表现出较好的焊缝成形.

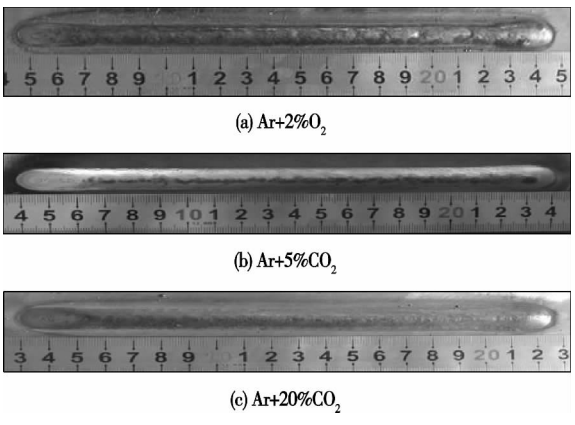

图 2 不同保护气体下焊缝成形

Fig. 2 Weld appearances with different atmosphere

2.2 微观组织

W1,W2 和 W3 分别为 Ar + 2% O_2,Ar + 5% CO_2 和 Ar + 20% CO_2 不同保护气体下的焊缝组织,图 3 为焊缝金相组织形貌(OM),由图 3 可以看出焊缝焊态组织为柱状晶,光学显微镜下可见明显的原奥氏体晶界(AGB),焊缝重热区为等轴晶,不同保护气体下焊缝金相组织均为贝氏体. 图 4 为焊缝组织 SEM 形貌,对比发现 W1 以粒状贝氏体为主,仅含有少量板条贝氏体,而 W2 和 W3 中板条贝氏体数量较多,且 W2 中可见排列较为规则的板条贝氏体,被粒状贝氏体挤压分割,呈细小板条束. 从图 4b W2 焊缝 SEM 形貌可以看出,在贝氏体区内,大量板条方向一致,贝氏体束相互平行,可有效提高焊缝韧性.

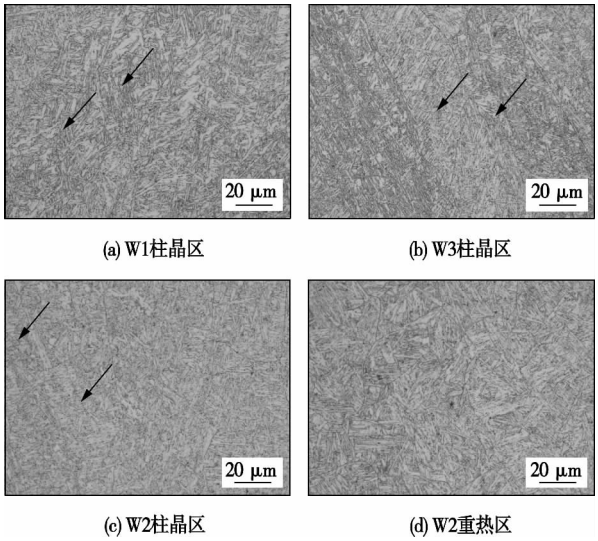

图 3 焊缝金相组织形貌(OM)

Fig. 3 OM images of microstructure of weld metals

从焊丝成分(表 1)可以看出,焊丝合金体系 Mn-Ni-Cr-Mo-Si-Ti 元素总含量提高,淬硬性增强,奥氏体向铁素体的转变被推迟,焊缝组织为中温转变组织. 粒状贝氏体主要由贝氏体铁素体板条及板条上的马氏体/奥氏体(M-A)小岛组成,焊缝组织在一定的连续冷却条件下,碳由 α/γ 相变前沿向 γ 内以较快速度扩散,避免了碳化物的析出,导致残余奥氏体中含碳量升高,奥氏体稳定性增强,随着组织进一步转变,将稳定的奥氏体包围,随后在冷却的过程中富碳奥氏体部分转变为马氏体,部分残留至室温以残余奥氏体形式存在,即形成 M-A. 图 4 为焊缝组织 SEM 形貌,可以看出整个视场内分布着许多白亮色 M-A 岛状物,岛形状极不规则,多呈棱角状或圆粒状,小尺寸岛状物细小弥散分布(图4b 中Ⅰ,Ⅱ),

但也存在某些少量较大呈块状 M-A 组元(图 4c 中Ⅲ) ，岛状物尺寸均小于 1 μm. M-A 组元为铁素体基体中的硬颗粒(低塑性相) ，试样受载时 M-A 组元阻碍铁素体中位错的运动，造成位错塞积，另外 M-A 组元与铁素体变形不协调，位错力与不协调力达到临界值便导致 M-A 组元开裂并形成微裂纹，外载荷进一步作用促使满足 Griffith 条件的微裂纹扩展进入铁素体基体，从而造成解理断裂. 相关研究表明[8,9] ，M-A 组元不同的形态及数量对于裂纹启裂的影响不同，颗粒状弥散分布的 M-A 不易使应力集中而诱发裂纹，而应变时块状的 M-A 组元与基体之间的界面上易成为启裂部位，萌生微空洞和微裂纹，即块状 M-A 数量增多，会使运行的位错在 M-A 组元与基体界面处大量塞积，加剧应力集中，使塑性的 α 相在变形时的滑移自由程减少，在低应力状态下导致基体分离而萌生为微裂纹，同时随着应力应变程度的增加，强烈的局部滑移作用也会导致条形或块状 M-A 自身发生开裂，随着外力或塑性变形继续增加，微裂纹通过彼此连接而扩展.

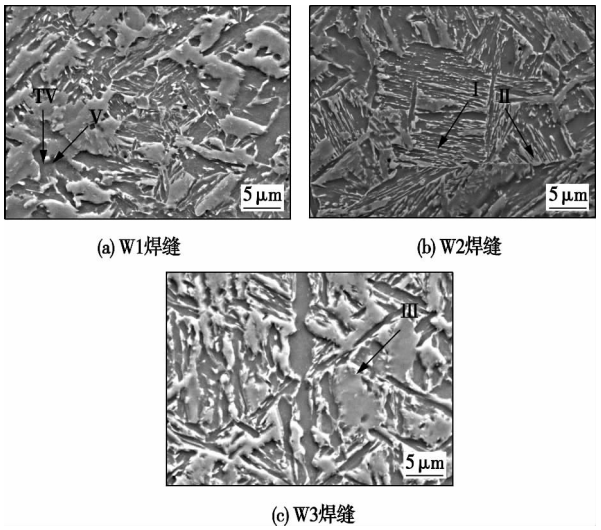

(a) W1焊缝　　(b) W2焊缝

(c) W3焊缝

图 4　焊缝组织 SEM 形貌

Fig. 4　SEM images of microstructure of weld metals

研究表明[10] 粒状贝氏体具有较大取向的晶畴尺寸，且粒状贝氏体中大角度晶界属于原始奥氏体晶界，当显微裂纹形成后大角度晶界可以使显微裂纹的扩展路径发生偏转而形成新的解理断裂小刻面，需消耗冲击吸收功. 分析认为粒状贝氏体为主的组织一般具有较好的韧性，但基体中的 M-A 组元数量和形态的差异会造成裂纹形核阶段冲击吸收功的不同. 对基体和焊缝中较大块状岛状物进行 EDS 分析，分析结果如表 3 所示. 结果表明，M-A 组元中存在 C 元素富集的现象，即 M-A 组元由富碳奥氏体转变形成. 相关研究表明[8,11] ，M-A 岛碳含量越高，对韧性的损害越大，因此为使熔敷金属获得较好的强韧性匹配，应严格控制焊丝中碳含量.

表 3　M-A 组元 EDS 成分分析(质量分数，%)

Table 3　Results of EDS analysis of M-A constituents

元素	W1 基体	W3 基体	岛状物Ⅲ	岛状物Ⅳ	岛状物Ⅴ
C	2.85	1.64	4.74	4.12	4.08
Si	0.74	1.42	1.13	1.17	1.02
Mn	1.57	2.33	1.59	1.76	1.99
Ni	1.93	2.52	2.49	2.79	2.43

2.3　力学性能

焊缝金属拉伸试验结果如表 4 所示，可见 W1 试样强度较低，CO_2 的加入后 W2 和 W3 试样强度提高，其中 W3 试样抗拉强度高达 950 MPa. 图 5 为熔敷金属冲击性能试验结果，可以看出 3 种试样的 -40 ℃冲击吸收功均大于 74 J，具有较好的冲击韧性. 采用 Ar + 5% CO_2 保护气体 W2 试样 - 60 ℃平均冲击吸收功为 72 J，冲击韧性最高，其次是 W3 试样，W1 试样冲击韧性最差. 分析认为 W1 焊缝金属组织主要由粒状贝氏体组成，W2 和 W3 焊缝金属组织则含有大量板条贝氏体，板条贝氏体可有效改善焊缝强韧性，因此 W2 和 W3 的强度和冲击吸收功均高于 W1. W2 贝氏体铁素体基体最细小，SEM 形貌可见大量平行排列的贝氏体条束，这对于提高韧性有利，同时 W2 中 M-A 岛多呈细小分布，对冲击韧

表 4　焊缝金属拉伸试验结果

Table 4　Results of tensile tests for weld metals

编号	保护气体	抗拉强度 R_m/MPa	屈服强度 R_{eL}/MPa	断后伸长率 A(%)
W1	Ar + 2% O_2	891	796	15.0
W2	Ar + 5% CO_2	926	836	18.0
W3	Ar + 20% CO_2	950	869	14.5

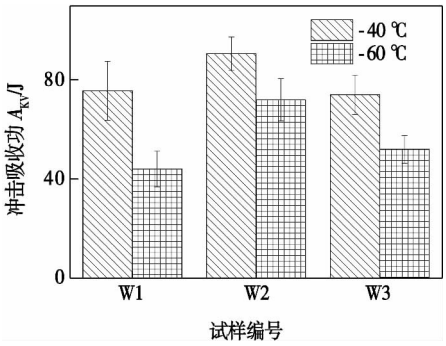

图 5　冲击吸收功试验结果

Fig. 5　Results of impact energy for weld metals

性的不利影响小，因此 W2 获得最佳强韧性匹配，而 W3 中少量块状分布的 M-A 岛存在，造成裂纹形核阶段冲击吸收功较低，对韧性不利，因此冲击吸收功明显低于 W2.

3 夹杂物分析

为进一步探究不同保护气体下焊缝冲击性能差异，采用 SEM 随机选取 50 个视场对焊缝中夹杂物的形貌与分布情况进行观察，并通过 Image-Pro Plus 软件对夹杂物进行统计分析. 结果表明夹杂物呈球形或椭球形，且随机分布在焊缝金属中. 图 6 为焊缝中夹杂物粒径分布直方图. 大量夹杂物 EDS 成分分析结果表明，3 种试样中夹杂物性质无明显区别，均为复合氧化物，且主要组成元素为 Mn-Si-Al-Ti-O. 由图 6 可见夹杂物直径较小且仅存在极少量大于 1 μm 的夹杂物，分布频率较高的尺寸范围集中在 0.2 ~ 0.4 μm. 对比发现 W1 焊缝中存在约 2% 的 0.8 ~ 1 μm 范围的较大尺寸夹杂物，W2 和 W3 焊缝中夹杂物尺寸均在 0.8 μm 以下，且 W2 焊缝中夹杂物的数量明显低于 W3 试样. 分析认为 3 种试样焊缝中夹杂物尺寸均较小，因此冲击韧性均较高，但采用不同比例保护气氛时，电弧氧化气氛存在差异，当焊缝中氧含量超过一定值，可能造成不利于韧性的大量氧化物生成，氧化物夹杂在晶界富集偏聚，造成晶界弱化，从而降低韧性. 分析认为保护气体变化，导致焊缝中夹杂物粒径分布出现差异，是造成冲击韧性不同的主要原因.

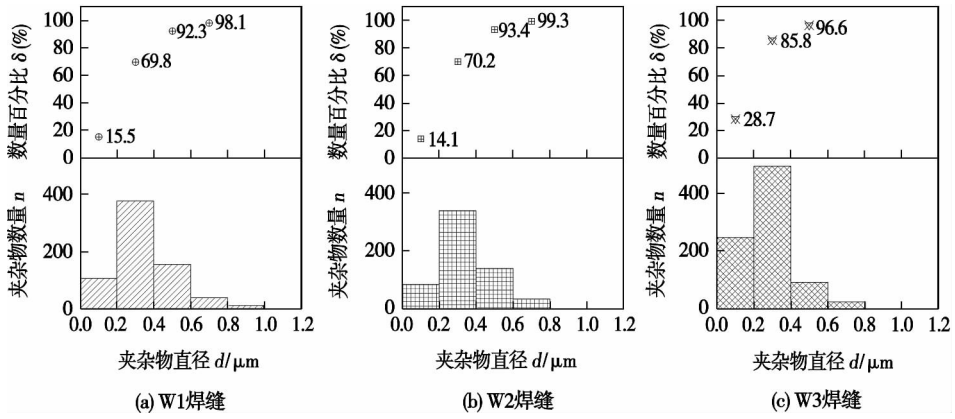

图 6 夹杂物粒径分布直方图

Fig. 6 Histogram of inclusion size distribution

4 断口形貌分析

冲击断口宏观形貌对比发现 W2 试样断口中放射区比例最小，纤维区和剪切唇比例较大，图 7 为 −60 ℃ 冲击断口裂纹扩展区 SEM 形貌，可以看出 3 种试样断裂机理不同. W1 试样和 W3 试样焊缝冲击断口呈现脆/韧混合断裂模式，断口中主要为呈准解理断裂特征的河流花样，且有少量的韧窝存在，其中 W3 试样断口裂纹扩展区存在少量韧窝，W3 焊缝则以准解理断口为主，仅存在极少量韧窝. W2 试样焊缝裂纹扩展区均为细小韧窝花样，韧窝具有一定的方向性，形状比较规则，分布较均匀，呈现韧性断裂模式. 高倍 SEM 下进一步观察发现断口韧窝底部一般含有较多颗粒状质点，EDS 成分分析表明，这些细小质点为焊接冶金反应过程中形成的氧化物夹杂，即说明延性韧窝为微孔聚集型机理. 由此可以

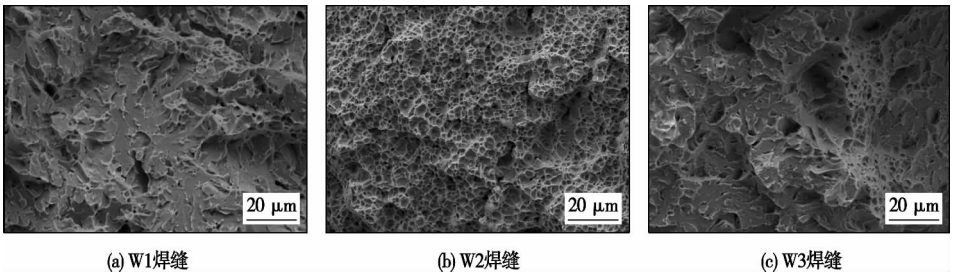

图 7 焊缝冲击断口 SEM 形貌

Fig. 7 SEM fractographs of impact fracture of weld metal

表明冲击断口形貌和冲击吸收功数值相吻合，保护气体变化导致冲击吸收功数值不同，冲击断口断裂模式也有所区别，不同保护气体下冲击断口由延性断裂转变为韧脆混合断裂，低温冲击韧性明显下降.

5　结　　论

(1) 针对该高强度气体保护焊焊丝，采用 Ar + 5% CO_2 保护气体，熔敷金属抗拉强度为 926 MPa，-60 ℃平均冲击吸收功为 72 J，强韧性最佳.

(2) 熔敷金属合金化程度提高，奥氏体转变被推迟，金相组织为中温转变组织粒状贝氏体 + 板条贝氏体，细小板条束存在可有效提高焊缝韧性; M-A 组元中存在明显 C 元素富集; 发生应变时，块状硬颗粒 M-A 组元易引起组元与基体界面处应力集中，诱发微裂纹，对韧性不利.

(3) 不同保护气体下熔敷金属中夹杂物尺寸均较小，但夹杂物粒径分布仍存在明显差异; 冲击吸收功的差异导致冲击断口形貌呈现出脆/韧混合断裂模式—韧性断裂模式.

参考文献:

[1] Thewlis G. Weldability of X100 linepipe [J]. Science and Technology of Welding and Joining, 2000, 5(6): 365 - 377.

[2] Luxenburger G, Bockelmann M, Wolf P. High strength quenched and tempered (Q + T) steels for pressure vessels [J]. Pressure Vessels and Piping, 2004, 81(2): 159 - 171.

[3] 铃木春义，田村博. 焊接金属学 [M]. 北京: 机械工业出版社, 1982.

[4] Huang Yamin, Wu Youming, Pan Chunxu. EBSD study of solidification characteristics of austenitic stainless steel weld pool [J]. Materials Science and Technology, 2010, 26(6): 750 - 753.

[5] 段旭东. 16Mn 钢混合气体保护焊时焊缝金属中气体含量变化的规律 [J]. 焊接学报, 2004, 25(5): 89 - 92.
Duan Xudong. Variational rule of gas content in 16Mn weld metal with mixed gas arc welding [J]. Transactions of the China Welding Institution, 2004, 25(5): 89 - 92.

[6] 张京海，魏金山，王雅升，等. 保护气体对焊缝金属氢脆敏感性影响的研究 [J]. 材料开发与应用, 2003, 18(5): 4 - 9.
Zhang Jinghai, Wei Jinshan, Wang Yasheng, *et al*. Effects of shielding gas on hydrogen embrittlement sensibility of deposit metal [J]. Development and Application of Materials, 2003, 18(5): 4 - 9.

[7] Basu B, Raman R. Microstructural variations in a high-strength structural steel weld inder isoheat input conditions [J]. Welding Journal, 2002, 81(11): 239 - 248.

[8] Bonneviea E, Ferrièrea G, Ikhlefa A, *et al*. Morphological aspects of martensite-austenite constitutes in intercritical and coarse grain heat affected zones of structural steels [J]. Materials Science and Engineering A, 2004, 385(1): 352 - 358.

[9] Hwang B, Kim Y G, Lee S, *et al*. Effective grain size andcharpy impact properties of high-toughness X70 pipeline steels [J]. Metallurgical and Materials Transactions A, 2005, 36(8): 2107 - 2114.

[10] Díaz-Fuentes M, Iza-mendia A, Gutiérrez I. Analysis of different acicular ferrite microstructures in low-carbon steels by electron backscattered diffraction. Study of their toughness behavior [J]. Metallurgical and Materials Transactions A, 2003, 34(11): 2505 - 2516.

[11] Chen J H, Kikuta Y, Araki T, *et al*. Micro-fracture behavior induced by M-A constituent (island martensite) in simulated welding heat affected zone of HT80 high strength low alloyed steel [J]. Acta Metallurgica, 1984, 32(10): 1779 - 1788.

作者简介: 吴炳智，男，1990 年出生，硕士研究生. 主要从事高强钢焊接材料和焊接工艺研究. 发表论文 1 篇. Email: bingzhw@gmail.com

chinery Company, Beijing 100076, China). pp 37 – 40

Abstract: LD10 aluminum alloy is mainly used in domestic aerospace vehicle propellant tank and mostly joined by TIG welding, and pores often appeared during fusion welding of aluminum alloy. This paper conducted TIG welding of 5.5 mm thick LD10 aluminum alloy plates with different welding parameters and calculated the porosity in the joints. The experimental results show that LD10 aluminum alloy joints made by TIG welding were prone to high porosity. The joints produced by double-faced three-pass welding technique had a higher unqualified rate after X-ray detection, but contained fewer micro-pores in the qualified ones. And micro-pores were much more easier to form in robot automatic welding than in manual welding. Porisity of the welds was 3.28%, 2.53%, 2.28% and 0.9%, respectively. During tensile test, cracks often generated at the pores in joints with high porosity.

Key words: LD10 aluminum alloy; TIG welding; porosity

Friction and wear properties of the zirconia coatings prepared by plasma spraying and laser remelting WANG Hongying, LI Zhijun, TANG Weijie, HAO Yunfei (Industrial Training Center, Shenzhen Polytechnic, Shenzhen 518055, China). pp 41 – 44

Abstract: The conventional and nanostructural zirconia coatings were prepared using plasma spraying, and then the nano zirconia coating was melted by laser. Friction and wear properties of conventional, nanostructural and laser remelted zirconia coatings were investigated at room and high temperatures. The experimental results show that the wear resistance properties of the nanostructural coating were obviously better than the conventional ones, and the nanostructural coating treated by laser remelting had the lowest friction coefficient and the best wear resistance. The analysis on surface micrographs of the three coatings shows that the surface roughness, porosity and cracking status were significantly different from each other, which resulted in a large difference in friction and wear properties for three zirconia coatings. The results indicate that nano powders plasma spraying, combining with laser remelting, was an effective approach to improve the performance of the zirconia coating.

Key words: plasma spraying; zirconia coating; laser remelting, friction and wear property

Dimensions optimization of ultra-high strength steel spot weld based on response surface methodology YU Huiping, WANG Weiwei, LIU Yuehua, LI Xiaoyang (College of Mechanical Engineering and Applied Electronics Technology, Beijing University of Technology, Beijing 100124, China). pp 45 – 48

Abstract: A parametric model for the tensile-shear spot welded structure of ultra-high strength steel was established with software ANSYS by APDL to analyze the static strength of the structure, and was verified with experiments. Based on the simulated results, the optimized model was built to decrease the whole materials, and some sizes of the structure were also optimized. The response surface methodology was adopted to make the stress constraints explicit, and the sequential quadratic programming algorithm was used to achieve the most suitable solutions of the optimized model. The results show that this method could effectively enhance the solving efficiency and avoid oscillation. The calculation procedure was programmed with C language in order to improve efficiency, and the results indicate that the optimization was feasible and effective.

Key words: ultra-high strength steel; spot-welded; dimensions optimization; response surface; sequential quadratic programming

Effect of filler metal on vacuum brazing of high volume fraction SiC_p/Al composites QI Junlei[1], WAN Yuhan[1], ZHANG Lixia[1], CAO Jian[1], FENG Jicai[1,2], LIANG Yingchun[3] (1. State Key Laboratory of Advanced Welding and Joining, Harbin Institute of Technology, Harbin 150001, China; 2. Shandong Provincial Key Laboratory of Special Welding Technology, Harbin Institute of Technology, Weihai 264209, China; 3. School of Mechatronics Engineering, Harbin Institute of Technology, Harbin 150001, China). pp 49 – 52

Abstract: Three different filler metals, Cu foil, Al-Si-Mg foil and Al-Si-Mg/Cu/Al-Si-Mg (ACA) composite foil, were used for vacuum brazing of 45% SiC_p/2024 Al composites. The microstructure of the interface in brazed seams was examined with SEM, EDS and XRD. And the effect of different filler metals on the interfacial microstructure and bonding strength was also analyzed. The formation of interface during vacuum brazing of 45% SiC_p/2024 Al composites with different filler metals and the fracture mechanism of the joint were revealed. The results indicate that ACA composite filler metal, combining the advantages of both Cu foil and AlSiMg foil, had lower liquidus temperature and better flowability. Through the diffusion of Cu atoms and prior eutectic reaction at the interface between aluminum alloy substrate and its oxide film, the removal ability of oxide film of the filler metal was enhanced and joining of 45% SiC_p/Al composites was achieved with high quality.

Key words: Al-based composite; vacuum brazing; composite material

Property and microstructure of deposited metal with high strength wire WU Bingzhi, XU Yujun, AN Hongliang, SUN Jingtao (Harbin Welding Institute, China Academy of Machinery Science & Technology, Harbin 150028, China). pp 53 – 57

Abstract: The microstructure and mechanical properties of deposited metal under different shielded gases were investigated by means of optical microscopy, scanning electron microscopy with EDS, tensile and impact tests. The results indicate that the best mechanical properties of deposited metal with the medium alloy solid wire were acquired when welded with Ar + 5% CO_2 mixed gas. The granular bainite dominated the microstructure of the deposited metal, and the existence of fine lath bainite improved the toughness effectively. In addition, carbon obviously enriched in M/A constituents, and massive M/A constituents could cause stress concentration by dislocation pile-up between M/A and base metal. Meanwhile, the micro crack appeared fre-

quently at the stage of crack nucleation. The increase of inclusions with large size was the main reason of the appearance of quasi-cleavage fracture and the decrease of impact absorbed energy.

Key words: high strength steel; deposited metal; mechanical property; microstructure

Influence of process parameters on the cracking rate and morphology of the laser melting and quenching zone in vermicular graphite cast iron ZHENG Ziyun, MA Bing, FENG Shengqiang, LIU Guang (Ningbo Branch of China Academy of Ordnance Science, Ningbo 315103, China). pp 58 – 62

Abstract: Laser melting and quenching experiments were conducted on vermicular graphite cast iron by employing 3 kW solid fiber laser. The cracking rate in the quenching zone, the morphology of the melting zone, microhardness and microstructure were analyzed. The results show that, at a given flow rate of shielding gas, increasing the laser power or reducing the scanning speed could facilitate the reduction of cracking rate in the quench zone. When the laser power was constant, the optimum flow rate of the shielding gas changed with the scanning speed. With the increase of laser power, the morphology of the quenching zone extended to the substrate. The morphology extended vertically and horizontally in the melting zone, and then in other directions. After that, it extended vertically and horizontally, and cycled. The gross area of the melting zone increased consequently, and the morphology of the quenching zone changed from flat to calyptra.

Key words: laser melting and quenching; vermicular graphite cast iron; cracking rate; melting zone; morphology

Microstructure characteristics of RuTi/1060Al fusion-brazed joint by pulsed gas metal arc welding WEI Shouzheng, LI Yajiang, WANG Juan, ZHANG Pengfei (Key Laboratory for Liquid-Solid Structural Evolution & Processing of Materials (Ministry of Education), Shandong University, Jinan 250061, China). pp 63 – 66

Abstract: Pulsed gas metal arc welding of RuTi titanium alloy to 1060 aluminum was conducted. The microstructure in weld zone of RuTi Ti/1060Al joint was examined by scanning electron microscope (SEM) fitted with energy-dispersive spectrometer (EDS). Elemental distribution and precipitated phase in weld zone and transition region on Ti alloy side were analyzed by EDS. The weld zone was composed of α-Al dendrites and eutectic α-Al + Si structures. The eutectic α-Al + Si structures distributed along the boundaries of α-Al dendrites. Striped or block $Ti(Al,Si)_3$ intermetallics appeared in the weld zone. A serrated transition region mainly containing $Ti(Al,Si)_3$ intermetallics was formed between the RuTi titanium alloy and the weld zone. The width of the Ti/Al transition region was less than 10 μm. With the increasing of welding heat input, the Ti/Al transition region presented a rod-like appearance. The heat-affected zone (HAZ) of RuTi titanium alloy consisted of acicular α″ and lath α′ martensite. The average microhardness in the HAZ was about 2.16 – 2.65 GPa.

Key words: RuTi titanium alloy; 1060 aluminum; pulsed gas metal arc welding; microstructure; precipitated phase

Uniform design and optimization of active flux for A-TIG welding of AZ31B magnesium alloy DU Xianchang, WANG Yi, GUO Shulan, YANG Chunguang (School of Mechanical and Electrical Engineering, Changchun Institute of Technology, Changchun 130012, China). pp 67 – 70

Abstract: Active fluxes with four components (TiO_2, $SrCl_2$, ZrO_2 and Y_2O_3) were developed based on the requirements of A-TIG welding of AZ31B magnesium alloy on active fluxes, including weld penetration, weld appearance, mechanical properties and reinforcement mechanism of weld, process feasibility and non-toxic etc. The composite active fluxes were designed by uniform design method. A mathematical model was established according to the weld penetration depth and weld appearance. The optimized ingredients of active fluxes were determined and verified through the comparative analysis with different mathematical models. The results show that the maximum penetration could be obtained with good weld appearance and the welded joint had excellent mechanical properties, when the active fluxes was designed with the proposed uniform design method.

Key words: magnesium alloy; active flux; uniform design

Analyses of reheat cracking sensitivity and test methods for 07MnNiVDR steel LIU Junsong[1,2], CHEN Xuedong[2], BU Huaquan[2] (1. School of Materials Science and Engineering, Hefei University of Technology, Hefei 230009, China; 2. Hefei General Machinery Research Institute, Hefei 230031, China). pp 71 – 74

Abstract: Reheat cracking sensitivity of the quenched and tempered high strength 07MnNiVDR steel was investigated with methods, such as low strain rate tensile test at high temperature after thermal simulation, Charpy pendulum impact test, implant test and small Tekken test. The thermal simulation results show that the steel was insensitive to reheat cracking with low welding heat input, but sensitive with high welding heat input and the sensitive temperature was around 600 ℃. Implant test also indicates that the steel had risk of reheat cracking to some extent, with sensitive temperature of about 600 ℃. The results of thermal simulation test and implant test were consistent with each other, while small Tekken test was not suitable for testing reheat cracking sensitivity. Low stain rate tensile test after thermal simulation was a practical and effective method for reheat cracking sensitivity assessment. The critical stress of implant test was important for engineering practice. Post-weld heat treatment of this steel joint should be prudent, although no apparent reheat cracking was found in small Tekken test.

Key words: high strength steel; reheat cracking; welding; thermal simulation

Spectral diagnostics of electron number density in plasma jet under atmosphere thermal plasma spray SUN Chengqi[1,2], GAO Yang[1], YANG Deming[1], CHEN Zhenyu[1] (1. School of Transportation Equipment and Ocean Engineering, Dalian Maritime University, Dalian 116026, China; 2. Maritime